
RH: An Architecture for Redesigning Quantum Circuits on Quantum Hardware Devices

Runhong He^{1*}, Ji Guan¹, Xin Hong¹, Xusheng Xu², Guolong Cui³,

Shengbin Wang⁴, Shenggang Ying^{1**}

* runhong93@qq.com

** sgying@ios.ac.cn

1. Key Laboratory of System Software (Chinese Academy of Sciences) and State Key Laboratory of Computer Science Institute of Software, Chinese Academy of Sciences, Beijing 100190, China
2. Beijing Academy of Quantum Information Sciences, Beijing 100193, China
3. Arclight Quantum Co., LTD. Chinese Academy of Sciences, Beijing 101408, China
4. China Telecom Quantum Information Technology Group Co., LTD, HeFei 233000, China

Abstract

In this paper we present an architecture that enables the redesign of large-scale quantum circuits on quantum hardware based on the entangling quantum generative adversarial network (EQ-GAN). Specifically, by prepending a random quantum circuit module to the standard EQ-GAN framework, we extend its capability from quantum state learning to unitary transformation learning. The completeness of this architecture is theoretically proved. Moreover, an efficient local random circuit is proposed, which significantly enhances the practicality of our architecture. For concreteness, we apply this architecture to three crucial applications in circuit optimization, including the equivalence checking of (non-) parameterized circuits, as well as the variational reconstruction of quantum circuits. The feasibility of our approach is demonstrated by excellent results in both classical and noisy intermediate-scale quantum (NISQ) hardware implementations. We believe our work will facilitate the implementation and validation of the advantages of quantum algorithms.

1 Introduction

Quantum algorithms can provide super-polynomial or even exponential speedups compared to their classical counterparts in solving certain important problems Nielsen and Chuang [2010], Bishnoi [2020], such as the large integers factoring Shor [1994], unstructured database searching Grover [1996], Long [2001] and linear systems solving Harrow et al. [2009], Wang et al. [2020]. Quantum algorithms are commonly represented as a certain quantum circuit comprised of a series of quantum gates. In the initial stage of quantum algorithm design, researchers tend to focus on functional specification, without giving significant consideration to actual implementation. Hence the resultant draft circuits may contain some logic operations, whose unitaries are known but whose implementations are not explicitly defined, such as the Oracles raised in the Grover’s algorithm Grover [1996], Long [2001]. Therefore, these high-level logic operations must be translated into the device’s native gate library for respecting hardware constraints – a process known as quantum logic circuit synthesis Ge et al. [2024]. In addition to manually performing it, which is a rather labor intensive and skill-demanding task in practice, some established techniques can also automatically

offer workable results, such as unitary decomposition Dawson and Nielsen [2005], Möttönen et al. [2004], genetic algorithm Williams and Gray [1998], evolutionary algorithm Ding et al. [2006], deep reinforcement learning Zhang et al. [2020], He et al. [2021], and variational quantum algorithm Rakyta and Zimborás [2022a,b], He et al. [2023].

Depending on their performance, various approaches might yield different results, resulting in the need to check the equivalence between their outputs. There are numerous algorithms that can do this, such as the decision graph Burgholzer and Wille [2020] for non-parameterized circuits and the ZX calculus Peham et al. [2023] for parameterized circuits. Unfortunately, their chief innovations might fail to work in certain cases, leaving the classical simulation to become the last resort. Suffering from the inefficient classical simulation of quantum systems this strategy scales very poorly with respect to the system’s size, and turn impractical as the number of qubits gets large. Thus it is highly desirable to establish an algorithm that do not suffer performance degradation as the involved qubits increase.

These problems are classically hard but quantumly easy. Reference Niu et al. [2022] proposes the entangling quantum generative adversarial algorithm (EQ-GAN) to reproduce a given reference quantum state based on quantum hardware Rasmussen and Zinner [2022]. It circumvents the classical simulation of quantum systems, and thereby can be applied to a large scale. The EQ-GAN can always converge to a provably optimal Nash equilibrium and avoids the mode collapse which may occur in traditional Q-GAN proposals Hu et al. [2019], Barbeau and Garcia-Alfaro [2019]. In addition, the EQ-GAN permits mitigating uncharacterized coherent error due to miscalibrated gate parameters. However, it cannot be directly used to redesign quantum circuits, because it actually learns only the first column of the corresponding unitary matrix. In our requirements, it is necessary to learn all elements of the unitary matrix.

Definition 1. *We define quantum circuit redesign as the task of transforming a given quantum circuit into an alternative circuit architecture while preserving its fundamental functionality.*

Many important applications fall naturally into the domain of quantum circuit redesign, such as the equivalence checking of quantum synthesized circuits, quantum circuits optimization and gate decomposition.

In this paper, we propose a novel approach which permits researchers to redesign large-scale quantum circuits on quantum hardware. We refer to this approach as the RH (Redesign circuits on quantum Hardware) architecture for simplicity. Our RH architecture contains and extends the EQ-GAN Niu et al. [2022], Rasmussen and Zinner [2022]. Specifically, by introducing an additional random quantum circuit module, the RH architecture can be directly applied to checking the equivalence between different circuits, whether they are parameterized or non-parameterized. Furthermore, this approach remains valid for variational learning of reference circuit functionality by structurally distinct parameterized circuits, owing to its inherent compatibility with quantum machine learning frameworks Benedetti et al. [2019]. The completeness of this architecture is theoretically proven. Moreover, an efficient local random circuit has been developed, which significantly enhances the practicality of this framework. To validate the RH architecture, we exemplarily implement three applications both in classical simulation and quantum hardware. Collectively these applications highlight the excellent performance of the RH architecture.

Our work opens a venue for redesigning quantum circuits using quantum hardware, permitting a wide range of applications such as large-scale quantum circuit optimization, equivalence checking, etc. It is important to highlight that our RH architecture can also be incorporated into other techniques for further advanced applications. For instance, it can be used to replace the classical simulation as the last resort, which is often the computational bottleneck, in some algorithms such as ZX Peham et al. [2023] and decision diagram Burgholzer and Wille [2020] for circuit simplification or optimization. We believe our RH architecture will facilitate the implementation and validation of advanced quantum algorithms.

2 Preliminaries

For readers’ convenience, this section introduces some quantum computation concepts central to our work. For additional quantum computing fundamentals, we refer readers to Reference Nielsen and Chuang [2010].

2.1 Quantum State and Quantum Circuit

In quantum computation, the fundamental unit of information is the quantum bit (qubit) - the quantum counterpart of the classical bit. The qubit's basis states $|0\rangle = [1, 0]^T$ and $|1\rangle = [0, 1]^T$ correspond to the classical 0 and 1 states, respectively. The essential quantum mechanical distinction is that a qubit can exist in any superposition of these basis states, described by: $|\psi\rangle = \alpha|0\rangle + \beta|1\rangle = [\alpha, \beta]^T$, where α and β are complex probability amplitudes obeying the normalization condition $|\alpha|^2 + |\beta|^2 = 1$. When measured, the qubit's superposition state collapses randomly to either $|0\rangle$ or $|1\rangle$, yielding either outcome 0 (with probability $|\alpha|^2$) or outcome 1 (with probability $|\beta|^2$). In Dirac notation, the bra state $\langle\psi|$ is defined as the Hermitian conjugate of the ket state $|\psi\rangle$, i.e., $\langle\psi| = (\langle\psi|)^\dagger = (\alpha^*, \beta^*)$. In an n -qubit system, the quantum state is spanned by a set of 2^n basis states. These basis states can be expressed as: $|x_1 x_2 \cdots x_n\rangle \equiv |x_1\rangle \otimes |x_2\rangle \otimes \cdots \otimes |x_n\rangle$, where $x_i \in \{0, 1\}$, and \otimes denotes the tensor product.

The overlap between two quantum states can be quantified by the fidelity $F = |\langle\psi'|\psi\rangle|^2$, which ranges from 0 (orthogonal states) to 1 (equivalent states). If two quantum states differ only by a global phase factor, namely, $|\phi\rangle = e^{i\theta}|\psi\rangle$ (where θ is a real phase angle), they are physically indistinguishable in all observable measurements and thus can be considered equivalent.

Quantum states are manipulated by quantum gates represented by unitary matrices U (where $U^\dagger U = I$). Any quantum logic operation can be realized by a circuit composed of arbitrary single-qubit rotation gates and at least one entangling two-qubit gate (e.g. CX or CZ).

2.2 SWAP Test

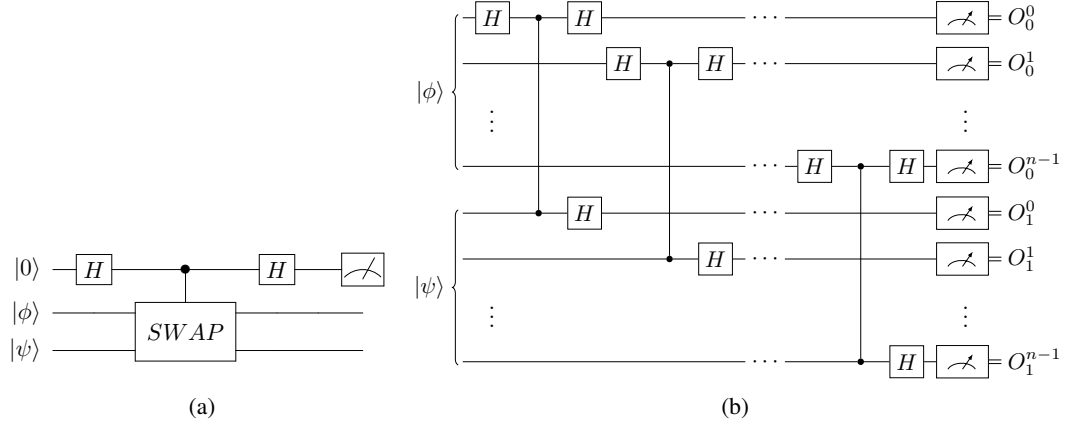


Figure 1: (a) The SWAP test circuit. (b) The destructive SWAP test circuit.

In the SWAP test Buhrman et al. [2001], whose circuit is visualized in Figure 1 (a), the measurement probability p_1 of obtaining outcome 1 on the ancillary qubit reflects the difference between input states $|\phi\rangle$ and $|\psi\rangle$ through the relation:

$$p_1 = \frac{1}{2} - \frac{1}{2}|\langle\phi|\psi\rangle|^2 = \frac{1}{2}(1 - F). \quad (1)$$

We define the probability of test failure as

$$p_{\text{failure}} = 2p_1 = 1 - F. \quad (2)$$

If the input states are equivalent, $p_{\text{failure}} = 0$; whereas for orthogonal states, p_{failure} reaches its maximum value of 1.

By simplifying the quantum circuit of the SWAP test, we can derive its destructive variant Garcia-Escartin and Chamorro-Posada [2013] (Figure 1 (b)). Here, the term “destructive” emphasizes the measurement-induced collapse of all data qubits' superposition states. The destructive SWAP test incurs no practical disadvantage compared to the standard version, as both protocols inherently consume the input states during measurement. In the destructive SWAP test, the parameter p_1 from

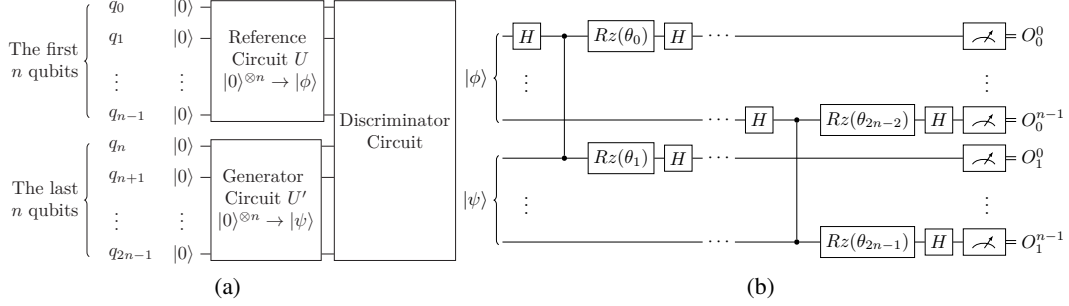


Figure 2: (a) The overall framework of the EQ-GAN algorithm Niu et al. [2022]. (b) The construction of discriminator in EQ-GAN Niu et al. [2022], Rasmussen and Zinner [2022].

the standard SWAP test is redefined as the probability of obtaining even results of $\sum_i O_0^i \& O_1^i$ on measurement outcomes, with symbol & referring to the AND operation Garcia-Escartin and Chamorro-Posada [2013].

2.3 EQ-GAN

The EQ-GAN algorithm Niu et al. [2022], Rasmussen and Zinner [2022] (Figure 2 (a)) is designed to reproduce a target quantum state $|\phi\rangle$ prepared by a reference circuit U on a parameterized generator circuit U' through variationally learning. A discriminator circuit evaluates the overlap between the target state $|\phi\rangle$ and the generator circuit's output state $|\psi\rangle$.

The destructive SWAP test can provide a perfect metric for states comparison in noise-free environments. Whereas in actual experiment, the two-qubit CZ gate on superconducting platform suffers from unstable coherent error due to miscalibrated gate parameters, which oscillate over the timescale of $O(10)$ minutes Arute et al. [2019]. To address this issue, EQ-GAN employs a parameterized destructive SWAP test as its discriminator, with the corresponding circuit implementation shown in Figure 2 (b). The coherent errors in CZ gates can be effectively compensated by subsequent single-qubit $R_z(\theta_i)$ gates with variationally optimized rotation angles θ_i Quantum et al. [2020], achieving high-fidelity SWAP test implementation in noisy environments. The generator circuit is then trained to minimize the discriminator's test failure probability until $p_{\text{failure}} \rightarrow 0$, indicating that the generator's output state $|\psi\rangle$ becomes equivalent to the target state $|\phi\rangle$ prepared by the reference circuit.

3 Proposed Method

3.1 Framework and Workflow

Our RH architecture is derived from the EQ-GAN Niu et al. [2022] and primarily consists of five components, as shown in Figure 3: two identical random circuits, one reference circuit U , one generator circuit U' and one discriminator circuit.

The heart of quantum circuit redesign lies in reproducing the functionality of a given n -qubit reference circuit by a n -qubit generator circuit with a new structure. To accomplish this, RH architecture need a $2n$ -qubit quantum system, where the reference circuit is deployed in the first n qubits while the generator circuit is located in the last n qubits. They transform the input random states $|\phi\rangle$ prepared by two identical random circuits into the states $|\phi\rangle$ and $|\psi\rangle$ respectively, and then feed them to the discriminator circuit. The discriminator circuit Niu et al. [2022] used here is the parameterized destructive SWAP test Garcia-Escartin and Chamorro-Posada [2013] (Figure 2 (b)), which quantifies the overlap between its input states $|\phi\rangle$ and $|\psi\rangle$. Specifically, the probability of test failure p_{failure} equals to the infidelity $1 - |\langle\phi|\psi\rangle|^2$, according to Equation (2). Thus, $|\phi\rangle$ is equivalent to $|\psi\rangle$ if $p_{\text{failure}} = 0$. In this case, we say the states pass the discriminator's test; otherwise, they fail the verification.

Our RH architecture begins by training the discriminator's parameters θ with two identical input states, i.e., $|\phi\rangle = |\psi\rangle$, aiming at minimizing the cost function p_{failure} . When $p_{\text{failure}} = 0$ the discriminator

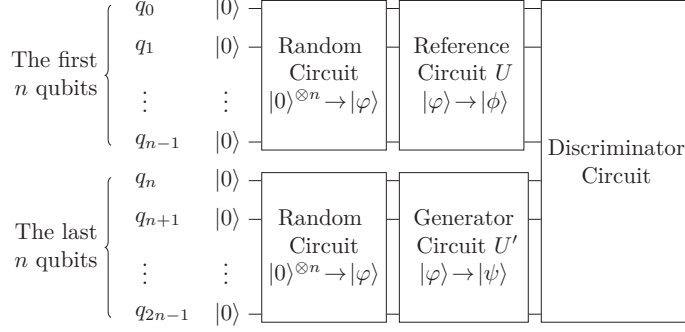


Figure 3: The schematic diagram of the RH architecture.

could act as a perfect destructive SWAP test under the influence of coherent error. Considering that the unique global optimum of the discriminator is to utterly eliminate the coherent error Niu et al. [2022] and any input states will lead to the same result, the zero state $|0\rangle^{\otimes n}$ is suitable for employment as the input states in training to reduce overhead. In other words, the random circuits, the reference circuit and the generator circuit can be ignored in this step.

Once a discriminator with well performance has been obtained after training, we can employ it to evaluate the overlap between the states generated by the reference and the generator circuits respectively. If the generator circuit is equivalent to the reference circuit, for any identical input $|\varphi\rangle$, their outputs should also be equivalent, and then pass the discriminator's test with $p_{\text{failure}} = 0$, i.e.,

$$p_{\text{failure}} = 1 - |\langle \phi | \psi \rangle|^2 = 1 - |\langle \varphi | U^\dagger U' | \varphi \rangle|^2 = 1 - |\langle \varphi | \varphi \rangle|^2 = 0. \quad (3)$$

Otherwise, p_{failure} will also reflect the overlap between two circuits, according to Equation (2).

3.2 Completeness and Limitations

We define the difference matrix to capture the error of the new circuit U' with respect to the target circuit U , which takes the form $D = U^\dagger U'$. The matrix D is also an unitary matrix, and will be an identity matrix \mathbb{I} if $U = U'$, i.e., these two circuits are equivalent. A non-identity D results from erroneous compilation of quantum gates in the new circuit U' .

In this paper, we employ random quantum states $|\varphi\rangle$ to conduct tests. According to the following Theorem 1, for several random states $|\varphi\rangle$, if the tests always yield the conclusion of equivalence between two circuits, i.e.,

$$1 = |\langle \varphi | U^\dagger U' | \varphi \rangle|^2 = |\langle \varphi | D | \varphi \rangle|^2 = |\langle \varphi | \varphi \rangle|^2, \quad (4)$$

the probability of that they are non-equivalence is statistically zero.

Theorem 1. *If $D|\varphi\rangle = |\varphi\rangle$ is satisfied for arbitrary random state $|\varphi\rangle$, D must be the identity matrix \mathbb{I} .*

Proof. Since $D|\varphi\rangle = |\varphi\rangle$, it follows that

$$\sum_j D_{i,j} |\varphi\rangle_j = |\varphi\rangle_i, \quad (5)$$

or

$$(D_{i,i} - 1) |\varphi\rangle_i = - \sum_{j \neq i} D_{i,j} |\varphi\rangle_j. \quad (6)$$

Given that $|\varphi\rangle$ is a random state with mutually independent components (disregarding the global factor), both sides of Equation (6) evaluate to 0. Therefore, $D_{i,i} = 1$ and $D_{i,j} = 0$ for any $j \neq i$, which implies that D is an identity matrix \mathbb{I} . \square

Clearly, any subtle distortion in the different matrix relative to the identity matrix will reduce the fidelity between the output states of the reference and generator circuits, consequently yielding a

non-zero p_{failure} through Equations (2) and (4). Therefore, the strategy of using random quantum states as inputs for both the reference and generator circuits, with equivalence checked by the discriminator, constitutes a theoretically complete verification framework. Another important reason for the adoption of random quantum states is that they lead to an open-loop training style for the subsequent generator optimization, reducing the susceptibility of the optimization to local optima akin to the usage of random samples in the training landscape of classical neural networks He et al. [2023], Goodfellow et al. [2016].

It should also be noted that as the number of qubits increases, the averaged probability amplitude of random quantum states decays exponentially across computational basis states. Consequently, in certain unfavorable scenarios the error detection probability becomes exponentially small. Assuming D includes only one non-trivial operation U_s , one of the worst-case scenarios occurs when this operation acts on the first qubit while being controlled by the remaining $n - 1$ qubits. The resulting difference matrix takes the form $D = \mathbb{I}_2^{\oplus(n-1)} \oplus U_s$, where \oplus denotes the direct sum operation of matrices. In this case, the probability that the error goes undetected within m measurement shots is about $e^{-m/2^{n-1}}$. However, for most cases, RH can detect the existence of errors within just a few thousand shots, as we will demonstrate in subsequent experiments, making it a valuable approach compared to classical simulation methods that fail to produce reference results for large-scale circuits within reasonable time. Furthermore, the RH framework can only probabilistically yield false negative conclusions (failing to detect actual differences between circuits) but is fundamentally impossible to produce false positives (where equivalent circuits are erroneously judged as non-equivalent) – assuming ideal operations and perfect measurements in experiment.

3.3 Efficient Local Random Circuit

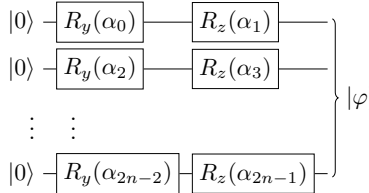


Figure 4: The local random circuit used in this paper.

Efficient and precise preparation of random quantum states constitutes a critical requirement for the practical implementation of the RH architecture. There are many approaches can be used to generate random quantum states. Such as the circuit whose gates are sampled and deployed randomly Boixo et al. [2018], and the amplitude encoding circuit Shende et al. [2005] whose parameters are randomly assigned. Nevertheless, these circuits are quite deep, especially the latter, which gives rise of exponential experimental cost. Here we devise a *local random circuit*, which is composed of a series of single-qubit rotation gates as illustrated in Figure 4 and generates quantum states that are the tensor product of n single-qubit random states from the initial state $|0\rangle^n$. The amplitude of the resultant local random state on the i^{th} computational basis is

$$|\varphi\rangle_i = \prod_{k=0}^{n-1} |\varphi_k\rangle_{\text{bin}(i)_k}, \quad (7)$$

where $|\varphi_k\rangle$ is the single-qubit random state encoded in the k^{th} qubit, and the function $\text{bin}(\cdot)$ outputs the binary representation of its input. The amplitudes are mutually independent (ignoring a trivial global normalization factor) as they differ by at least one random number, thereby fulfilling the prerequisites for applying Theorem 1.

It worth stating that although this circuit cannot generate truly entangled states, they will *arithmetically* exist as components in a certain amount in the resultant states. For example, $(|00\rangle + |01\rangle + |10\rangle + |11\rangle)/2$ can be viewed arithmetically as a superposition of entangled states $(|00\rangle + |11\rangle)/\sqrt{2}$ and $(|01\rangle + |10\rangle)/\sqrt{2}$.

4 Experiments

Many important applications are naturally categorized as quantum circuit redesign problems. For the sake of concreteness, we apply our RH architecture to three applications: non-parameterized (and parameterized) quantum circuit equivalence checking, and quantum circuit variational reconstruction. These applications capture the core of quantum circuit redesign and simultaneously are limited to a small-scale (4-qubit) to be performable by current quantum devices. Larger-scale validation experiments ($4 \sim 9$ qubits) based purely on classical simulation are presented in Appendix A.2. To assess the performance of the RH architecture, we conduct these applications both in numerical

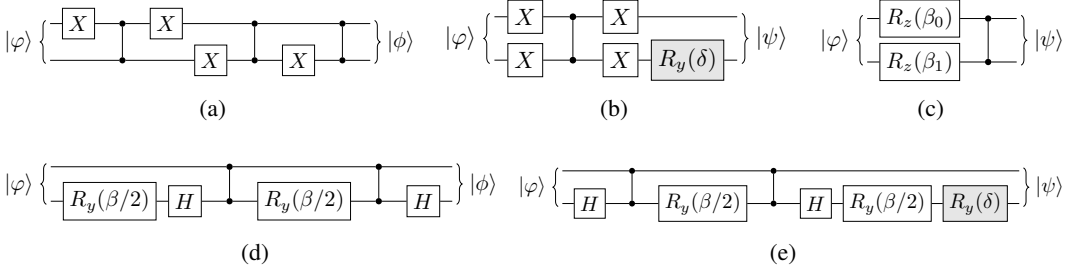


Figure 5: (a) A two-qubit phase-flipper circuit for basis states $|01\rangle$, $|10\rangle$ and $|11\rangle$. (b) A two-qubit phase-flipper circuit for basis state $|00\rangle$. (c) A potential alternative to the circuit (a) implemented by one two-qubit CZ gate and two single-qubit rotation gates. (d) and (e) are two decomposition circuits which are frequently employed for implementing the $CR_y(\theta)$ gate. The gray $R_y(\delta)$ gates in circuits (b) and (e) are introduced to create a controlled amount of distortion relative to their original functionality.

simulation and in current NISQ hardware devices. The numerical simulation is performed with Python 3.10, MindSpore Quantum 0.10 Xu et al. [2024] and have been run on an 4-core 1.8 GHz CPU with 8 GB memory. The hardware experiments are carried out on the Zuchongzhi-2 quantum processor, a 66-qubit superconducting quantum platform that was used to demonstrate quantum advantage Zhu et al. [2022]. Detailed hardware experiment information, including error rates and qubit-mapping schematic, is provided in Appendix A.1. The code and data used in this paper are publicly available on Gitee at https://gitee.com/mindspore/mindquantum/tree/research/paper_with_code.

4.1 Preliminary Experiment

Before implementing these applications, we first train the discriminator circuit – a 4-qubit parameterized destructive SWAP test circuit Garcia-Escartin and Chamorro-Posada [2013] (Figure 2 (b)). For training the discriminator efficiently, we feed it two zero states, i.e. $|\psi\rangle = |\phi\rangle = |\varphi\rangle = |0\rangle^{\otimes 2}$ with reasons explained in Subsection 3.1, and optimize its parameters θ to minimize the p_{failure} , allowing it to eventually act as an effective destructive SWAP test circuit in a noisy environment. The well trained discriminator obtained here will be reused in following applications.

To evaluate the discriminator’s robustness against errors, we introduce two additional R_z gates (not shown in the figure) after each CZ gate in the classical simulation, modeling the effect of coherent errors Niu et al. [2022]. The parameters of these R_z gates are randomly sampled from a normal distribution with $\mu = 0$ and $\sigma = 0.02$. The discriminator’s trainable parameters θ are initialized to zero and optimized using the Adam optimizer with an initial learning rate of 0.1. When all parameters $\theta = 0$, the parameterized discriminator degenerated into the original destructive SWAP test.

In Figure 6 (a), we depict the evolution of the cost function p_{failure} with respect to the training steps in training the discriminator classically. We can see that within 500 training steps the probability of test failure gradually decreases, from the initial value of 3.148×10^{-4} to a minimum of 2.232×10^{-17} . In hardware experiment, the p_{failure} decreases from the initial 9.400×10^{-2} to a minimum of 5.150×10^{-2} within 50 training steps (without presenting in figure). The number of shots in experiment is 1000 throughout this paper.

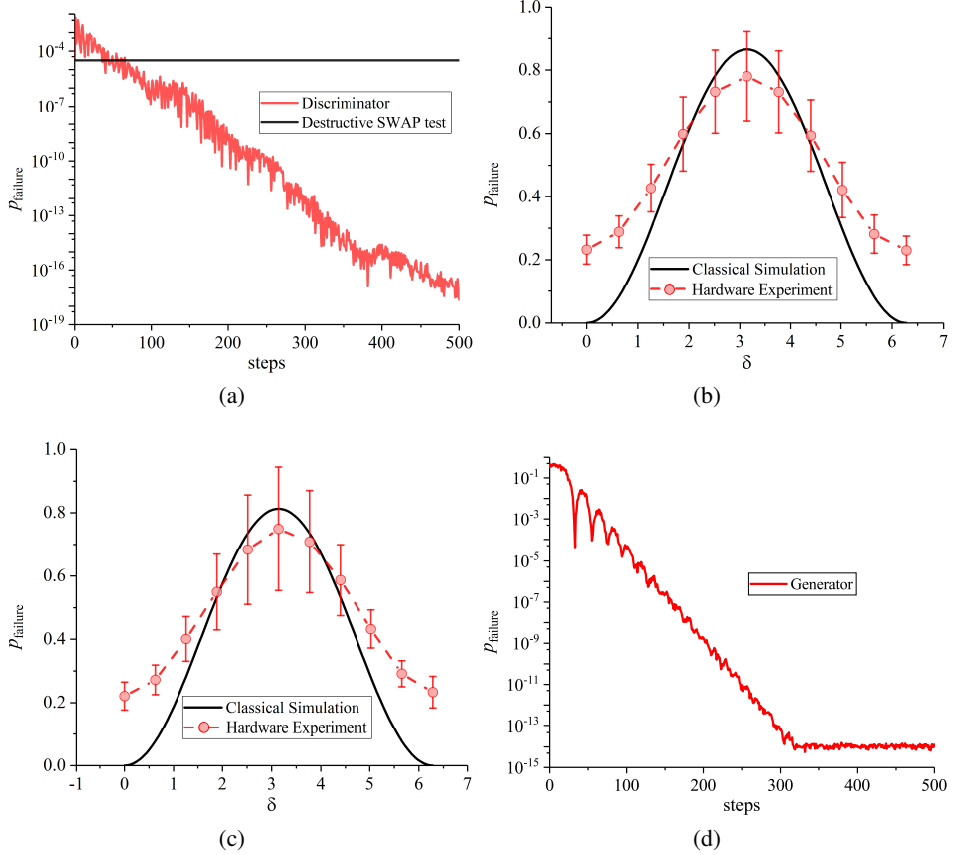


Figure 6: (a) The probabilities of test failure as functions of steps in training the discriminator classically. (b) The averaged probabilities of test failure (with ± 1 standard deviation error bars) vary with the value of parameter δ in the circuit of Figure 5 (b). (c) The averaged probabilities of test failure (with ± 1 standard deviation error bars) exhibit a parametric dependence on δ in the circuit of Figure 5 (e). (d) The averaged probability of test failure evolves with respect to the training steps in classical simulation.

Table 1: The comparison of the discriminator's performance before and after training, along with the values of its parameters. The notation θ refers to the results from classical simulation, while θ^* refers to the results from hardware experiment.

p_{failure}	i	0	1	2	3
1.291×10^{-3}	θ	0.0	0.0	0.0	0.0
1.214×10^{-9}	θ	4.981×10^{-3}	-1.088×10^{-2}	6.910×10^{-3}	-8.094×10^{-3}
9.104×10^{-2}	θ^*	0.0	0.0	0.0	0.0
7.862×10^{-2}	θ^*	1.692×10^{-2}	1.618×10^{-2}	-1.114×10^{-2}	5.916×10^{-2}
—	error	-4.981×10^{-3}	1.088×10^{-2}	-6.910×10^{-3}	8.093×10^{-3}

In Table 1, we record the performance comparison of the discriminator before and after training, as well as the values of its parameters. Referring to Table 1, after training, not only the discriminator reduces the probability of test failure from 1.291×10^{-3} to 1.214×10^{-9} in simulation, but also the optimized parameters perfectly compensate for the randomly instantiated coherent error which is listed in the last row, i.e. $\theta_i = -\text{noise}_i$, achieving perfect error cancellation. These results indicate that the discriminator actually acquires remarkable error robustness by training. We emphasize here that during the training process, the p_{failure} is calculated for zero states, while in the final performance evaluation in Table 1, the p_{failure} is averaged over 100 random quantum states. Their specific values might vary, yet the main conclusion holds.

4.2 Application 1: Non-parameterized Quantum Circuit Equivalence Checking

The first application to be outlined is checking the equivalence between two non-parameterized circuits. We take the circuits shown in Figure 5 (a) and (b) as the reference circuit and the generator circuit in RH architecture respectively. Ignoring the $R_y(\delta)$ gate in gray, these two circuits are phase-flippers and have important applications in oracle-based quantum algorithms, such as the Grover’s searching algorithm Grover [1996]. When $\delta = 2k\pi$ (k is an integer), these two structurally distinct circuits are equivalent up to a global phase -1 , and thus may be generated by different synthesis tools for the same unitary matrix. The necessity of carrying out an equivalence checking on them naturally arises. To achieve this, we take 100 random states $|\varphi\rangle$ as inputs and study the averaged probability of test failure as the parameter δ of the R_y gate in gray alters.

From Figure 6 (b), we see that as δ increases within the interval $[0, 2\pi]$, the probability of test failure first rises from 0 and then falls back, which precisely conforms to the theoretical expectations. Similar conclusion can also be drawn according to the hardware results, albeit with deviations caused by noise and operational imperfections.

4.3 Application 2: Parameterized Circuit Equivalence Checking

Owing to the current prevalence of quantum machine learning, checking the equivalence of parameterized circuits is a highly important but simultaneously intractable problem, and there is a lack of universal and effective solutions Peham et al. [2023]. In this Subsection, as a representative example, we consider the equivalence checking between two decomposition circuits of the $CR_y(\beta)$ gate, which are shown in Figure 5 (d) and (e), respectively. These two parameterized circuits are equivalent for any real β when the parameter of the $R_y(\delta)$ gate in gray satisfies $\delta = 2k\pi$, where k is an integer, and deviates from each other in other cases.

Figure 6 (c) describes the averaged p_{failure} in classical simulation and hardware experiment over 10 random states and 10 random β in terms of the value of δ in the interval $[0, 2\pi]$. The feasibility of checking equivalence between parameterized circuits with random free parameters, i.e., the β herein, has been proven in Reference Peham et al. [2023]. It can be concluded from Figure 6 (c) that the probabilities of test failure nicely reflect the amount of deviation between the two circuits as the δ varies.

4.4 Application 3: Quantum Circuit Variational Optimization

Circuit optimization seeks to construct equivalent quantum circuits with either reduced gate counts or shallower depths compared to their target circuits. For complex circuit optimization, variational algorithms often provide more reliable and systematic approaches than developer intuition alone He et al. [2023].

The example we present here is to reduce the depth of a particular circuit illustrated in Figure 5 (a) in a variational manner. A potential alternate is depicted in Figure 5 (c), which comprises two single-qubit R_z gates with trainable parameters β_0 and β_1 , as well as one CZ gate. Within the RH architecture, we designate these two circuits as the reference circuit and the generator circuit respectively. In this example, the settings of the hyper-parameters are aligned with those in the previous training of the discriminator, such as the parameters initialization, learning rate, cost function and so on.

Figure 6 (d) reveals that as the training steps increasing, the p_{failure} in classical simulation steadily decreases from an initial value of 6.654×10^{-1} and converges to around 1×10^{-14} after about 300 steps. The results from hardware experiment show that the probability of test failure has declined from the initial value of 8.66×10^{-1} to a minimum of 1.099×10^{-1} during a 50-step training procedure (without presenting in figure). The p_{failure} during training is dynamically computed using a batch of 4 random states. These observations imply that the RH architecture works well in this application, and the resultant generator circuit can be a competent alternative to the reference circuit in experiment after training.

5 Conclusion

In this paper, we formally defined the task of quantum circuit redesign, and introduced a novel RH architecture for redesigning large-size quantum circuits on quantum hardware that overcomes

the classical simulation bottleneck inherent to existing methods. The RH architecture is built upon the EQ-GAN, and extends its capability from quantum states learning to unitary transformation learning by inserting a quantum random circuit module prior to it. We proposed the usage of $|0\rangle^n$ state in training the discriminator to minimize resource overhead and error accumulation, and demonstrated the discriminator’s robustness against coherent errors of CZ gate on superconducting quantum processors. We proved the RH architecture’s completeness and discussed its limitations. An efficient local random quantum circuit was developed that drastically slashes implementation overhead, boosting practical utility. As demonstrations, we implemented the RH architecture to three critical applications: (non) parameterized circuit equivalence checking and variational reconstruction of quantum circuits. Evaluation results from both classical simulation and quantum hardware experiments confirm the superior performance of the RH architecture.

The RH architecture is also compatible with other existing circuit optimization techniques like ZX-calculus, enabling collaborative solutions for advanced circuit optimization challenges. We believe our RH architecture could help boost innovation in designing advanced quantum circuits.

References

Frank Arute, Kunal Arya, Ryan Babbush, Dave Bacon, Joseph C Bardin, Rami Barends, Rupak Biswas, Sergio Boixo, Fernando GSL Brandao, David A Buell, et al. Quantum supremacy using a programmable superconducting processor. *Nature*, 574(7779):505–510, 2019. URL <https://doi.org/10.1038/s41586-019-1666-5>.

Michel Barbeau and Joaquin Garcia-Alfaro. Faking and discriminating the navigation data of a micro aerial vehicle using quantum generative adversarial networks. In *2019 IEEE Globecom Workshops (GC Wkshps)*, pages 1–6. IEEE, 2019.

Marcello Benedetti, Erika Lloyd, Stefan Sack, and Mattia Fiorentini. Parameterized quantum circuits as machine learning models. *Quantum Science and Technology*, 4(4):043001, 2019.

Bhupesh Bishnoi. Quantum computation. *arXiv preprint arXiv:2006.02799*, 2020. URL <https://arxiv.org/abs/2006.02799>.

Sergio Boixo, Sergei V Isakov, Vadim N Smelyanskiy, Ryan Babbush, Nan Ding, Zhang Jiang, Michael J Bremner, John M Martinis, and Hartmut Neven. Characterizing quantum supremacy in near-term devices. *Nature Physics*, 14(6):595–600, 2018. URL <https://doi.org/10.1038/s41567-018-0124-x>.

Harry Buhrman, Richard Cleve, John Watrous, and Ronald De Wolf. Quantum fingerprinting. *Physical review letters*, 87(16):167902, 2001.

Lukas Burgholzer and Robert Wille. Advanced equivalence checking for quantum circuits. *IEEE Transactions on Computer-Aided Design of Integrated Circuits and Systems*, 40(9):1810–1824, 2020.

Kean Chen, Wang Fang, Ji Guan, Xin Hong, Mingyu Huang, Junyi Liu, Qisheng Wang, and Mingsheng Ying. Veriqbench: A benchmark for multiple types of quantum circuits, 2022. URL <https://arxiv.org/abs/2206.10880>.

Christopher M Dawson and Michael A Nielsen. The solovay-kitaev algorithm. *arXiv preprint quant-ph/0505030*, 2005. URL <https://arxiv.org/abs/quant-ph/0505030>.

Shengchao Ding, Zhi Jin, and Qing Yang. Evolving quantum oracles with hybrid quantum-inspired evolutionary algorithm, 2006. URL <https://arxiv.org/abs/quant-ph/0610105>.

Juan Carlos Garcia-Escartin and Pedro Chamorro-Posada. Swap test and hong-ou-mandel effect are equivalent. *Physical Review A*, 87(5):052330, 2013.

Yan Ge, Wu Wenjie, Chen Yuheng, Pan Kaisen, Lu Xudong, Zhou Zixiang, Wang Yuhan, Wang Ruocheng, and Yan Junchi. Quantum circuit synthesis and compilation optimization: Overview and prospects. *arXiv preprint arXiv:2407.00736*, 2024.

Ian Goodfellow, Yoshua Bengio, and Aaron Courville. *Deep Learning*. The MIT Press, USA, 2016.
ISBN 0262035618.

Lov K Grover. A fast quantum mechanical algorithm for database search. In *Proceedings of the twenty-eighth annual ACM symposium on Theory of computing*, pages 212–219, 1996.

Aram W Harrow, Avinatan Hassidim, and Seth Lloyd. Quantum algorithm for linear systems of equations. *Physical review letters*, 103(15):150502, 2009.

Run-Hong He, Rui Wang, Jing Wu, Shen-Shuang Nie, Jia-Hui Zhang, and Zhao-Ming Wang. Deep reinforcement learning for universal quantum state preparation via dynamic pulse control, 2021.
URL <https://doi.org/10.1140/epjqt/s40507-021-00119-6>.

Run-Hong He, Xu-Sheng Xu, Mark S Byrd, and Zhao-Ming Wang. Modularized and scalable compilation for double quantum dot quantum computing. *Quantum Science and Technology*, 9(1):015004, oct 2023. doi: 10.1088/2058-9565/acfe38. URL <https://dx.doi.org/10.1088/2058-9565/acfe38>.

Ling Hu, Shu-Hao Wu, Weizhou Cai, Yuwei Ma, Xianghao Mu, Yuan Xu, Haiyan Wang, Yipu Song, Dong-Ling Deng, Chang-Ling Zou, et al. Quantum generative adversarial learning in a superconducting quantum circuit. *Science advances*, 5(1):eaav2761, 2019.

Gui-Lu Long. Grover algorithm with zero theoretical failure rate. *Physical Review A*, 64(2):022307, 2001.

Mikko Möttönen, Juha J Vartiainen, Ville Bergholm, and Martti M Salomaa. Quantum circuits for general multiqubit gates. *Physical review letters*, 93(13):130502, 2004.

Michael A Nielsen and Isaac L Chuang. *Quantum Computation and Quantum Information 10th Anniversary Edition*. Cambridge University Press, 2010.

Murphy Yuezhen Niu, Alexander Zlokapa, Michael Broughton, Sergio Boixo, Masoud Mohseni, Vadim Smelyanskyi, and Hartmut Neven. Entangling quantum generative adversarial networks. *Physical Review Letters*, 128(22):220505, 2022.

Tom Peham, Lukas Burgholzer, and Robert Wille. Equivalence checking of parameterized quantum circuits: Verifying the compilation of variational quantum algorithms. In *Proceedings of the 28th Asia and South Pacific Design Automation Conference*, pages 702–708, 2023.

Google AI Quantum, Collaborators*†, Frank Arute, Kunal Arya, Ryan Babbush, Dave Bacon, Joseph C Bardin, Rami Barends, Sergio Boixo, Michael Broughton, Bob B Buckley, et al. Hartree-fock on a superconducting qubit quantum computer. *Science*, 369(6507):1084–1089, 2020.

Péter Rakyta and Zoltán Zimborás. Approaching the theoretical limit in quantum gate decomposition. *Quantum*, 6:710, 2022a.

Péter Rakyta and Zoltán Zimborás. Efficient quantum gate decomposition via adaptive circuit compression. *arXiv preprint arXiv:2203.04426*, 2022b.

SE Rasmussen and NT Zinner. Multiqubit state learning with entangling quantum generative adversarial networks. *Physical Review A*, 106(3):032429, 2022.

Vivek V Shende, Stephen S Bullock, and Igor L Markov. Synthesis of quantum logic circuits. In *Proceedings of the 2005 Asia and South Pacific Design Automation Conference*, pages 272–275, 2005.

Peter W Shor. Algorithms for quantum computation: discrete logarithms and factoring. In *Proceedings 35th annual symposium on foundations of computer science*, pages 124–134. Ieee, 1994.

Shengbin Wang, Zhimin Wang, Wendong Li, Lixin Fan, Zhiqiang Wei, and Yongjian Gu. Quantum fast poisson solver: the algorithm and complete and modular circuit design. *Quantum Information Processing*, 19:1–25, 2020.

Colin P Williams and Alexander G Gray. Automated design of quantum circuits. In *NASA International Conference on Quantum Computing and Quantum Communications*, pages 113–125. Springer, 1998.

Xusheng Xu, Jiangyu Cui, Zidong Cui, Runhong He, Qingyu Li, Xiaowei Li, Yanling Lin, Jiale Liu, Wuxin Liu, Jiale Lu, Maolin Luo, Chufan Lyu, Shijie Pan, Mosharev Pavel, Runqiu Shu, Jialiang Tang, Ruqian Xu, Shu Xu, Kang Yang, Fan Yu, Qingguo Zeng, Haiying Zhao, Qiang Zheng, Junyuan Zhou, Xu Zhou, Yikang Zhu, Zuoheng Zou, Abolfazl Bayat, Xi Cao, Wei Cui, Zhendong Li, Guilu Long, Zhaofeng Su, Xiaoting Wang, Zizhu Wang, Shijie Wei, Re-Bing Wu, Pan Zhang, and Man-Hong Yung. Mindspore quantum: A user-friendly, high-performance, and ai-compatible quantum computing framework, 2024. URL <https://arxiv.org/abs/2406.17248>.

Yuan-Hang Zhang, Pei-Lin Zheng, Yi Zhang, and Dong-Ling Deng. Topological quantum compiling with reinforcement learning. *Physical Review Letters*, 125(17):170501, 2020.

Qingling Zhu, Sirui Cao, Fusheng Chen, Ming-Cheng Chen, Xiawei Chen, Tung-Hsun Chung, Hui Deng, Yajie Du, Daojin Fan, Ming Gong, Cheng Guo, Chu Guo, Shaojun Guo, Lianchen Han, Linyin Hong, He-Liang Huang, Yong-Heng Huo, Liping Li, Na Li, Shaowei Li, Yuan Li, Futian Liang, Chun Lin, Jin Lin, Haoran Qian, Dan Qiao, Hao Rong, Hong Su, Lihua Sun, Liangyuan Wang, Shiyu Wang, Dachao Wu, Yulin Wu, Yu Xu, Kai Yan, Weifeng Yang, Yang Yang, Yangsen Ye, Jianghan Yin, Chong Ying, Jiale Yu, Chen Zha, Cha Zhang, Haibin Zhang, Kaili Zhang, Yiming Zhang, Han Zhao, Youwei Zhao, Liang Zhou, Chao-Yang Lu, Cheng-Zhi Peng, Xiaobo Zhu, and Jian-Wei Pan. Quantum computational advantage via 60-qubit 24-cycle random circuit sampling. *Science Bulletin*, 67(3):240–245, 2022. ISSN 2095-9273. doi: <https://doi.org/10.1016/j.scib.2021.10.017>. URL <https://www.sciencedirect.com/science/article/pii/S2095927321006733>.

A Technical Appendices and Supplementary Material

A.1 Hardware Information

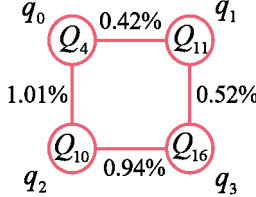


Figure 7: The mapping schematic between the logical qubits and the physical qubits arranged in a 2×2 sub-grid within the Zuchongzhi-2 quantum processor. The hardware was calibrated on December 11th, 2024.

To access results from quantum hardware, we map the utilized 4 logical qubits q_i onto physical qubits Q_i in a 2×2 sub-grid of the 66-qubit Zuchongzhi-2 quantum processor for accommodating the experimental realities. The mapping diagram is illustrated in Figure 7 (c), where the label of line between physical qubits indicates the error rate in executing CZ gate. The error rates of single-qubit native gates are between 0.11% and 0.21%, and the average readout error rate is 4.21%.

A.2 Advanced Experiments

In Section 4, we demonstrated the workflow of our RH architecture through three small-scale proof-of-concept experiments. We now consider larger-scale scenarios. Since quantum circuit equivalence verification constitutes the core contribution of the RH framework and serves as the foundation for all its applications, this section focuses on benchmarking its performance for various commonly used quantum circuits. The benchmark circuits are selected from the VeriQBench dataset Chen et al. [2022], covering major quantum computing applications, such as the quantum machine learning, variational quantum computational chemistry, Grover’s algorithm, quantum fourier transform, qubit mapping and quantum volume tests, etc.

Given current quantum hardware’s noise limitations for deep multi-qubit circuits, we restrict our benchmarking to only classical simulations. The tested circuits are limited to $n = 4 \sim 9$ qubits (RH architecture: $2n = 8 \sim 18$ qubits) to comply with the computational constraints of classical simulators. We stress that the RH architecture is theoretically scalable to arbitrary circuit sizes. With anticipated advancements in quantum hardware, particularly fault-tolerant quantum computers, verification of circuits comprising hundreds to thousands of qubits will become experimentally feasible.

To evaluate RH’s performance, we prepare generator circuits by inserting quantum gates at random positions in given reference circuits. We generate equivalent circuit by inserting an identity gate into the given reference circuit, while creating non-equivalent circuit through the insertion of $R_x(1.23)$ rotation gate. As for the parameterized circuits, such as the ‘qaoa_6’ and ‘qcnn_4’, we randomly instantiate their parameters, as justified by the theoretical proof in Reference Peham et al. [2023].

The benchmark results are summarized in Table 2, where $p_{\text{failure_Y}}$ denotes the test failure probability for equivalent circuit pairs and $p_{\text{failure_N}}$ represents the failure probability for non-equivalent pairs under the RH architecture, respectively.

As evidenced by the benchmark data in Table 2, the test failure probability $p_{\text{failure_Y}}$ remains zero within machine precision ($\sim 10^{-31}$) for equivalent circuit pairs. In contrast, for non-equivalent pairs, the test failure probability $p_{\text{failure_N}}$ ranges from 0.155 to 0.329, implying the non-equivalence between these circuits can be readily detected by the RH.

Table 2: Benchmark results for quantum circuit equivalence checking using VeriQ Bench dataset Chen et al. [2022].

Benchmark	<i>n</i>	#gates	#depth	$p_{\text{failure_Y}}$	$p_{\text{failure_N}}$	<i>t</i> [s]
2of5d2	7	12	8	1.511×10^{-31}	0.322	1.503
2of5d3	6	137	65	3.620×10^{-31}	0.307	0.466
3_17tc	3	6	5	4.220×10^{-32}	0.253	0.068
4b15g_4	4	45	24	1.113×10^{-31}	0.279	0.086
4b15g_5	4	15	12	2.169×10^{-32}	0.252	0.073
4_49_fc	4	143	72	3.267×10^{-31}	0.279	0.158
adder_n4	4	4	4	6.765×10^{-32}	0.293	0.100
adder_n7	7	8	5	1.531×10^{-31}	0.328	1.658
bv_4	4	12	3	1.307×10^{-31}	0.181	0.107
bv_5	5	15	4	1.843×10^{-31}	0.191	0.145
bv_7	7	21	6	2.751×10^{-31}	0.264	2.369
bv_9	9	27	8	3.777×10^{-31}	0.250	6.587
eff_4_4	4	19	3	1.115×10^{-31}	0.312	0.184
eff_5_4	4	19	3	1.025×10^{-31}	0.243	0.146
grover_5	5	23	4	2.269×10^{-31}	0.291	0.1815
grover_7	7	32	8	3.146×10^{-31}	0.252	2.8121
grover_9	9	41	12	3.999×10^{-31}	0.167	7.702
ham7tc	7	143	71	4.279×10^{-31}	0.219	7.520
hf_6_0_9	6	155	32	6.389×10^{-31}	0.155	0.805
hwb4_11_21	4	11	10	7.354×10^{-32}	0.312	0.072
mod5d1	5	8	8	9.571×10^{-32}	0.303	0.116
nth_prime4_inc_d1	4	72	38	1.696×10^{-31}	0.221	0.126
nth_prime7_inc_1427_3172	7	2513	1566	3.358×10^{-30}	0.329	111.947
pe_4	5	18	9	1.865×10^{-31}	0.284	0.181
pe_5	6	25	12	2.465×10^{-31}	0.172	0.316
pe_7	8	42	18	3.698×10^{-31}	0.287	3.711
pe_8	9	52	21	4.324×10^{-31}	0.160	11.118
qaoa_6	6	110	9	4.668×10^{-31}	0.260	0.830
qcnn_4	4	66	16	4.056×10^{-31}	0.208	0.264
qft_4	4	10	5	1.178×10^{-31}	0.243	0.102
qft_5	5	15	7	1.630×10^{-31}	0.265	0.188
qft_7	7	28	11	2.602×10^{-31}	0.260	2.818
qft_9	9	45	15	3.691×10^{-31}	0.183	11.671
rand_cliff_4_AG	4	25	9	1.490×10^{-31}	0.166	0.122
rand_cliff_7_AG	7	83	46	2.729×10^{-31}	0.313	5.268
rand_cliff_8_AG	8	108	59	3.505×10^{-31}	0.270	9.386
rand_cliff_9_AG	9	107	61	3.820×10^{-31}	0.326	22.744
rd32	4	4	4	7.213×10^{-32}	0.252	0.084
5QBT_4CYC_4GN_1.0P2_0	4	4	4	7.154×10^{-32}	0.315	0.096
16QBT_4CYC_8GN_1.0P2_0	9	8	1	2.169×10^{-31}	0.306	5.236
20QBT_4CYC_8GN_1.0P2_0	5	8	3	1.150×10^{-31}	0.250	0.115
54QBT_4CYC_8GN_1.0P2_0	8	8	1	1.856×10^{-31}	0.250	1.983
quantum_volume_n5_d5_i0	5	100	15	8.247×10^{-31}	0.298	0.363
quantum_volume_n7_d5_i0	7	150	15	1.271×10^{-30}	0.291	9.102
quantum_volume_n9_d5_i0	9	200	15	1.716×10^{-30}	0.155	43.420

n: Number of qubits #gates: Number of gates #depth: Circuit depth

$p_{\text{failure_Y}}$: p_{failure} for equivalent circuits $p_{\text{failure_N}}$: p_{failure} for non-equivalent circuits

t: The total runtime for 100 parameter instances..